

Metal Crystal/Polycrystal Plasticity and Strengths

Ronald W. Armstrong 

Department of Mechanical Engineering, University of Maryland, College Park, MD 20742, USA; rona@umd.edu

Abstract: A brief historical sketch is given of Taylor's dislocation density-based model description, leading to the prediction of a parabolic, tensile, stress–strain curve for the plastic deformation of aluminum. The present focus is on additional results or analyses obtained on the subject for crystal/polycrystal strain hardening. Our current understanding of such material behavior is attributed to post-Taylor descriptions of sequential deformation stages in stress–strain measurements that are closely tied to specific dislocation interaction and reaction mechanisms. A schematic comparison is given for individual face-centered cubic (fcc), body-centered cubic (bcc), and hexagonal close-packed (hcp) crystal curves and to related strength properties determined for individual crystals and polycrystalline material. For the fcc case, an example sessile dislocation reaction is described based on a stereographic projection. Then, quantitative constitutive-relation-based assessments are presented for the tensile strain hardening leading to the plastic instability behaviors of copper and tantalum materials.

Keywords: Taylor-based strain hardening; crystal plastic deformation stages; deformation-induced dislocation interactions/reactions; polycrystal tensile plastic instability

1. Introduction

Soon after crystal dislocations were invented on an atomic lattice basis in 1934, G.I. Taylor produced a dislocation model calculation that allowed him to obtain parabolic strain hardening in a tensile stress (σ_ϵ)–strain (ϵ) curve for the 20th century face-centered cubic (fcc) metal: aluminum [1]. Not much changed on the subject until 1951, when another dislocation inventor, Orowan, stated that “Since the publication of Taylor's (1934) theory there has been no significant progress in the understanding of strain hardening” [2,3]. The sentiment was repeated years later by Cottrell [4], as recently quoted [5]. The present report aims to refute this claim by providing an update on the enhanced knowledge gained over these many years about the dislocation mechanics of plastic deformation, particularly of plastic strain hardening.

The 1950s signaled the beginning of an explosion in dislocation observations, particularly by Hirsch and colleagues [6] with the transmission electron microscope (TEM) and through dislocation associations made with a broad range of mechanical properties being measured comprehensively for fcc, body-centered cubic (bcc) and hexagonal close-packed (hcp) metals. An early sign of progress on strain hardening was reported in the 1960 TMS Institute of Metals Lecture given by Mott [7]. Additional mechanical property measurements/analyses that have been achieved until the present time are included in the present report. Not least are advances made in the development of computationally based metal constitutive relations for determining the full σ_ϵ – ϵ behavior and of experimental and simulated crystal/polycrystal deformations.

2. Stress–Strain Characterizations of Fcc, Bcc and Hcp Metal Deformations

Post-Taylor description of the several topics, such as dislocation line intersections; partial dislocations and associated stacking faults; slip plane changes through cross-slip; solute pinning of individual dislocations; and grouped dislocation pile-up mechanisms, were soon associated with the three-crystal-structure-type deformations. Figure 1 shows schematic shear stress (τ_ϵ)–shear strain (γ) curves for the crystal structure types in which particular



Citation: Armstrong, R.W. Metal Crystal/Polycrystal Plasticity and Strengths. *Metals* **2022**, *12*, 2070. <https://doi.org/10.3390/met12122070>

Received: 8 November 2022

Accepted: 14 November 2022

Published: 1 December 2022

Publisher's Note: MDPI stays neutral with regard to jurisdictional claims in published maps and institutional affiliations.



Copyright: © 2022 by the author. Licensee MDPI, Basel, Switzerland. This article is an open access article distributed under the terms and conditions of the Creative Commons Attribution (CC BY) license (<https://creativecommons.org/licenses/by/4.0/>).

regions of the deformation curves are marked either with subscript athermal or thermal dependencies, so also being dependent on the imposed metal strain rate in shear, $(d\gamma/dt)_\epsilon$.

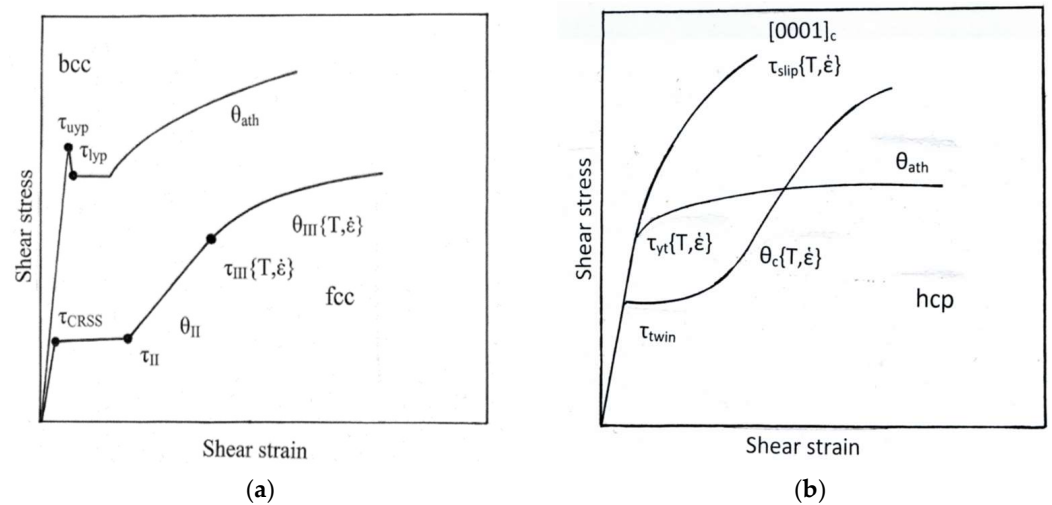


Figure 1. Schematic single-crystal resolved shear stress (τ) versus resolved shear strain (γ) for bcc (a) and hcp (b) crystal structure types.

The interstitial solute pinning of dislocations produces the indicated upper and lower yield point behavior for the bcc curve in Figure 1a, whereas the subsequent plastic strain hardening, $(d\gamma/dt)_\epsilon = \theta_{ath}$, is essentially athermal. The bcc yield stress, with or without a yield point, exhibits a strong thermal dependence. In contrast, multiple stages are also shown in Figure 1a for the fcc curve corresponding to the initial yielding on a single-slip system in stage I, then moving to the activation of double-slip systems in stage II, followed by the advent of cross-slipping in stage III. Stage I for aluminum is normally mostly absent and the combination of θ_{ii} and θ_{iii} stages approximate to the parabolic strain hardening produced in the Taylor model. The latter two stages are more clearly identified for copper, as explained on the basis of a higher stacking fault energy for aluminum providing smaller partial dislocation separations and, hence, easier cross-slip [8].

The schematic curves for the hcp crystal case in Figure 1b show a significant variation because of the restricted distribution of available slip (or deformation twinning) systems and the significantly different shear stress levels required for their operation, whether in tension or compression. In the case of magnesium, for example, the highest critical resolved shear stress, τ_{CRSS} , is obtained for the compression of a single crystal along the [0001] direction for pyramidal slip, and the lowest shear stress for the initial deformation twinning of a polycrystal that transitions at larger strain to an analogous steeper strain hardening for pyramidal (and prism) slip is also obtained [9]. An intermediate thermally dependent shear stress at yield, $\tau_{yt}\{T, [d\epsilon/dt]\}$, and athermal strain hardening, θ_{ath} , is shown to be bcc-like for an AZ31B magnesium alloy (0001)-plane textured sheet material subjected to in-plane tension tests [10]. Xie, Zhu, Kang and Yu have presented model constitutive relations for extruded AZ31B material under tensile (θ_{ath}) and compressive (θ_c) loading conditions [11].

3. Dislocation Interactions/Reactions

An early post-Taylor investigation of the thermal dependence of stage I, “easy glide”, in (hcp) magnesium single crystals led to the interpretation of dislocation ‘forest’ intersections controlling the rate dependence of plastic flow [12]. Dislocation ‘jogs’ and point defects are generated for the further passage of the otherwise mobile dislocations. The same mechanism carries over for the fcc single-crystal stage I case to stage II, in which exceptional hardening is produced by dislocation interactions at slip plane intersections. An important element of the hardening is attributed to dislocation reactions that occur along combined line length segments of the intersecting dislocations. The basis for the reacted dislocations is their relatively lower self-energies compared to the paired dislocation reactants [13].

Hirth provided a detailed geometric description of the possible dislocation reactions for the fcc case [14]. Figure 2 is a stereographic projection that has been constructed to show the particular case described by Hirth for $[\bar{1}10](111)$ and $[011](\bar{1}\bar{1}1)$ slip system intersections to produce hardening via a sessile “stair rod” dislocation obstacle. For the bcc case, reacted sessile $[100]$ Burgers vector dislocations are produced and are made even more complicated for multiple sessile dislocation reactions produced in hcp crystal deformations involving the basal, pyramidal and prism slip systems.

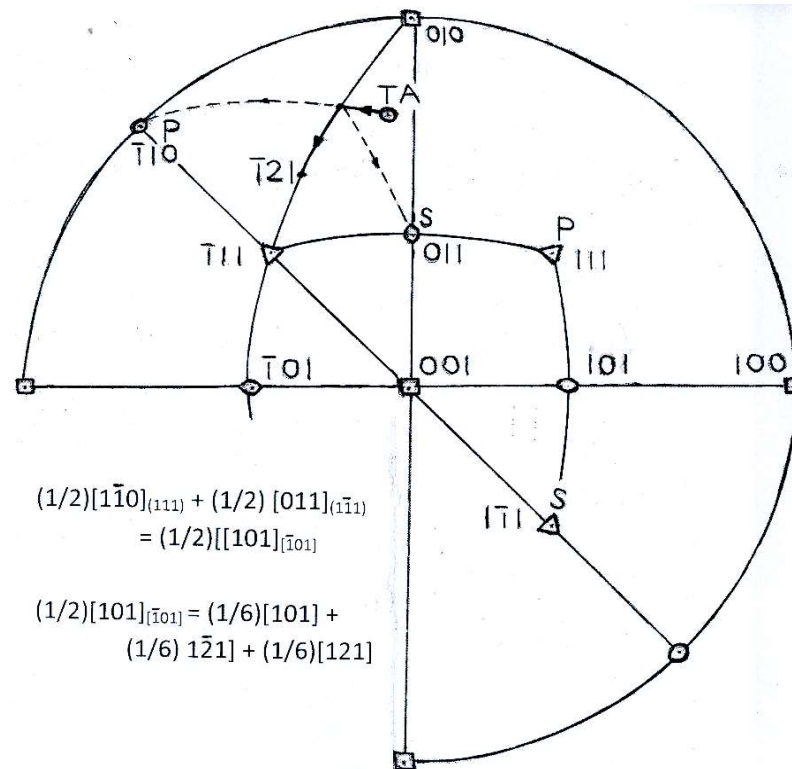


Figure 2. Stereographic projection for tensile axis (TA) rotation associated with the start of stage I type $[\bar{1}10]$ slip on the (111) primary slip plane (P), then leading to stage II rotation with addition of $[011]$ slip on the secondary $(\bar{1}\bar{1}1)$ slip plane (S), for which a sessile “stair rod” dislocation obstacle, among other partial dislocations, is produced with Burgers vector, $(1/6)a[101]$, and line direction along $[\bar{1}01]$.

4. Strain Hardening and (Tensile) Plastic Instability

A seemingly minor influence of the polycrystal grain size on the tensile plastic deformation of aluminum, an effect that had been missed by Taylor, was established in the pioneering work by Hansen [15]. A later report by Hansen and Ralph established a stronger grain size effect for copper [16]. In both cases, the grain size effect was explained in terms of an analogous and much stronger grain size dependence reported in the early 1950s for α -iron and steel materials by Hall [17] and by Petch [18], respectively. The grain size effect was attributed to dislocation pile-ups in slip bands being needed to overcome the grain boundary’s resistance to the transmission of plastic flow between the grains within a polycrystal. A constitutive relation incorporating the grain size effect for polycrystalline copper was originally reported by Zerilli and Armstrong [19] and was updated by Zerilli [20] as follows:

$$\sigma_\varepsilon = \sigma_{0G\varepsilon} + B_0[\varepsilon_r(1 - \exp\{\varepsilon/\varepsilon_r\})]^{1/2}(\exp[-\alpha T]) + k_\varepsilon \ell^{-1/2} \quad (1)$$

In Equation (1), $\sigma_{0G\varepsilon}$ is an athermal stress; B_0 is the thermal stress at absolute temperature, $T = 0$; and $k_\varepsilon \ell^{-1/2}$ is the Hall–Petch term for an inverse square root of the grain diameter, $\ell^{-1/2}$, multiplied by the stress intensity parameter, k_ε ; ε_r is a recovery strain; and $\alpha = \alpha_0 - \alpha_1 \ln(d\varepsilon/dt)$ for a coupled T and strain rate dependence. The first two terms on the

right side of Equation (1) are normally combined in the single Hall–Petch intercept stress, $\sigma_{0\epsilon}$. Under small strain, a Taylor-type parabolic stress–strain dependence is obtained.

Figure 3 provides an assessment of the strain-hardening behavior able to be derived from the Hansen and Ralph investigation of copper $\sigma_\epsilon - \epsilon$ behavior in tension and leading to a grain size dependence of the plastic instability condition based on the Considère relationship: $\sigma_\epsilon = (d\sigma_\epsilon / d\epsilon)$ at the tensile maximum load point. For the copper material (and many other metals), the tensile strain hardening was found to be contained in $(d\sigma_{0\epsilon} / d\epsilon)$, while k_ϵ was constant at $\sim 5 \text{ MPa}\cdot\text{mm}^{1/2}$. The product $B\exp(-\alpha T) = B' = 500 \text{ MPa}$ was determined for $\sigma_{0\epsilon}$ from the experimental strain dependence of $\sigma_{0\epsilon}$, thus providing for the assumption of $\sigma_{0G\epsilon} = 0$. The value of ϵ_r was estimated as 1.2, and its influence on the deviation of the $\sigma_\epsilon - \epsilon$ curve from the Taylor prediction is shown to begin at $\epsilon = \sim 0.15$ for material with a $40 \mu\text{m}$ grain size. Otherwise, a comparison of the computed curves for the 4.0 and $40 \mu\text{m}$ grain size curves shows that plastic instability occurs sooner for material with a smaller grain size. The computations are consistent with a limiting value of $\epsilon = 0.3$ reported by Hansen and Ralph for their highest uniform tensile strain measurements.

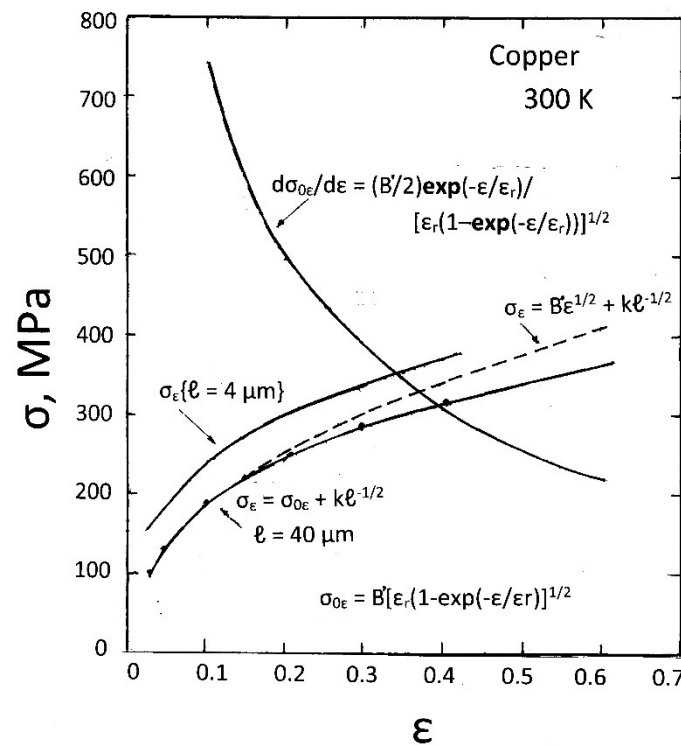


Figure 3. Computations specifying the maximum uniform strain achieved in tension for copper material measurements reported on a Hall–Petch basis by Hansen and Ralph [16]; in the figure, $B' = B\exp[-\alpha T]$.

5. Plastic Instability for the Bcc Case

The following constitutive relation has been validated for bcc ARMCO iron material [19]:

$$\sigma_\epsilon = \sigma_{0G\epsilon} + B_0\exp(-\beta T) + A\epsilon^n + k_\epsilon\epsilon^{-1/2} \tag{2}$$

In Equation (2), $\sigma_{0G\epsilon}$ is an analogous athermal stress component to that described for Equation (1); B_0 is the thermal stress at $T = 0$; $\beta = \beta_0 - \beta_1\ln(d\epsilon/dt)$ as for the α parameter in Equation (1); and A and n are constants measuring the material strain hardening. Thus, again, the first three terms in Equation (2) are an expanded interpretation of $\sigma_{0\epsilon}$ as for Equation (1). It is of particular note that the bcc $(d\epsilon/dt)$ and T dependencies are in the yield stress, while the strain hardening is essentially athermal.

Beyond the evaluation of the constants in Equation (2) for ARMCO iron material, an extensive investigation was conducted for a wide range of experimental measurements

reported for tantalum materials [21]. In particular, Hoge and Mukherjee had reported complete $\sigma_\varepsilon - \varepsilon$ measurements over a wide range of T and strain rates [22]. Figure 4 provides a summary description for the application of Equation (2) to describe the accumulated measurements. In the figure, $c_0 = \sigma_{0G\varepsilon}$ and $K = A$. One might note that the $n = 0.44$ value in the figure is close to the Taylor specification. Otherwise, the locus for the maximum load point for the Hoge and Mukherjee measurements is seen to follow an essentially athermal strain hardening behavior, in line with the designation in the Figure 1 schematic.

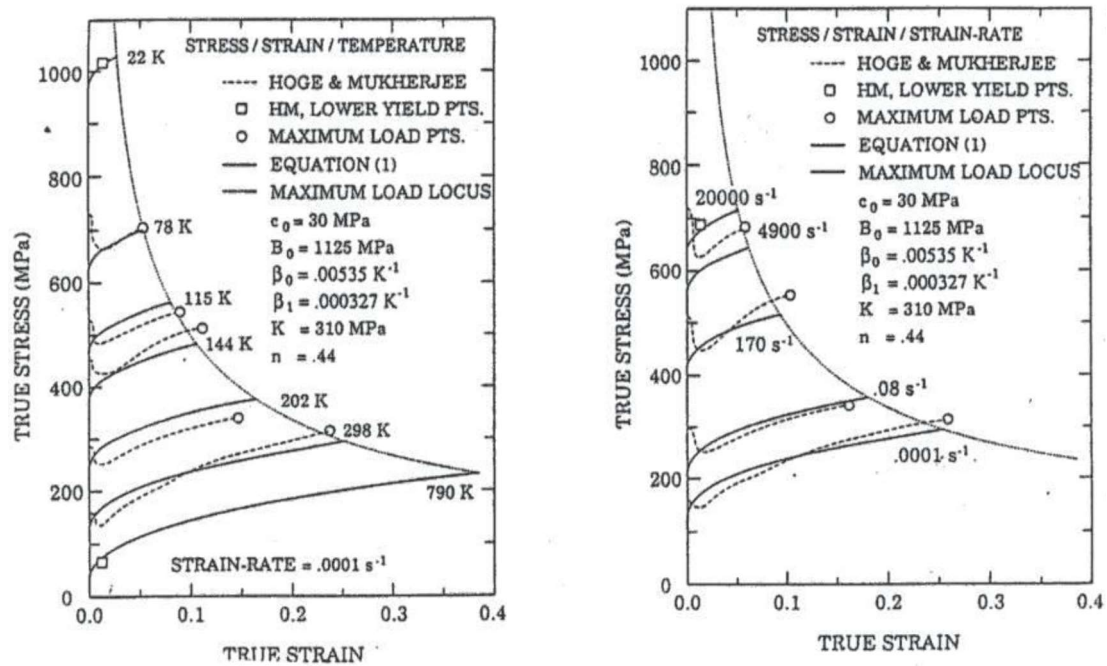


Figure 4. Stress–strain measurements obtained over a wide range of temperatures and strain rates for tantalum by Hoge and Mukherjee [22], as shown to be describable on a bcc constitutive relation basis [21], shown in combined form with permission from AIP Publishing, 2022.

6. Discussion

The preceding description of strength and strain hardening measurements and their analyses on a dislocation mechanics basis provides evidence of progress made in understanding crystal/polycrystal plasticity carrying on from the outstanding work performed by Taylor. Here, additional references are added to provide further evidence for the increased understanding being brought to bear on the subject.

Peeters, Bacroix, Teodosiu, Van Houtte and Aernoudt have monitored via TEM the dislocation densities within slip bands of individual grains in an interstitial-free (IF) polycrystalline iron material and correlated the measurements with an extension of the Taylor model [23]. Messemaeker, Verlinden and Van Humbeeck presented measurements influenced by the complementary grain boundary, for which the generated dislocation densities were contained in $\sigma_{0\varepsilon}$ and thus implicitly contain the influence of strain hardening [24]. Madec and Kubin reported on both bcc and fcc dislocation reactions occurring during straining [25], while Messner, Rhee, Arsenlis and Barton attributed strain hardening in the hcp lattice to dislocation reaction (junctions) occurring in accordance with the Frank and Nicholas dislocation self-energies [13,26]. Most recently, Mishra and Alankar have applied discrete dislocation dynamics for plastic deformation of copper being controlled by the formation of dislocation reacted junctions and cross-slip [27].

An interesting report made by Li, Cui, Yan, Zhang et al. put forth the suggestion for additive manufacturing that the dislocation cell walls formed at larger deformation are anchored by reacted sessile dislocations and thereby require small dislocation pile-ups for breaching [28]. Such model consideration relates to the subject of deformation structures induced by severe plastic deformation, for example, as reported by Muñoz, Higuera and

Cabrera for ARMCO iron material deformed to additional stages IV and V by equal-channel angular pressing (ECAP) [29]. The measurements were analyzed in relation to accumulated dislocation measurements and to a Hall–Petch grain size description.

Lastly, there is mention of a relationship between $\sigma_\varepsilon - \varepsilon$ behavior and other properties, for example, fatigue and hardness behaviors. Brown has given emphasis to the importance of the thermally activated annihilation of screw dislocation dipoles at the endurance limit measured in fatigue tests of copper, thus establishing a relationship with strain hardening in stages III and IV of tensile tests [30]. In further work connecting the strain hardening and fatigue behavior of fcc crystals, emphasis was given to understanding the role of dislocation mechanisms at the slip band level [31]. Alhafez, Ruestes, Bringa and Urbassek reported quantitative counts of $(a/2) \langle 111 \rangle$ slip and $a \langle 100 \rangle$ -reacted Burgers-vector dislocations produced within the plastic deformation zones of simulated nano-indentations made in a (001) α -iron crystal surface [32]. Goel, Cross, Stukowski, Gamsjäger, Beake and Agrawal demonstrated that $a[100]$ reacted dislocation line lengths formed at the earliest stages of deformation in simulations of nano-indentations made in tungsten crystals [33]. Armstrong and Elban have reported comparative plastic strain hardening behaviors in post-pop-in plastic deformation at nano-indentations and in drawn wire and micro-pillar deformation tests [34].

7. Summary

A brief description has been given, first, of the important impetus given by Taylor of understanding the nature of crystal plasticity, particularly connecting with an understanding of crystal strain hardening. Subsequent developments of the dislocation mechanics of the subject have been reviewed, with focus on further refinements in dislocation model developments, for example: the role of crystal deformation for partial dislocations and stacking faults; dislocation interactions/reactions and cross-slips; metal grain size; and crystal/polycrystal stress–strain applications, including their tensile plastic instability properties and grouped dislocation behaviors in slip band stress concentrations.

Funding: This research received no external funding.

Acknowledgments: Appreciation is expressed for the correspondence with Yuri Estrin, Alexei Vinogradov and Dierk Raabe on the subject of the present report.

Conflicts of Interest: The author declares no conflict of interest.

References

1. Taylor, G.I. The Mechanism of Plastic Deformation of Crystals. *Part I. Theoretical*. *Proc. R. Soc. Lond.* **1934**, *145*, 362–387.
2. Nabarro, F.R.N.; Basinski, Z.S.; Holt, D.B. The plasticity of pure single crystals. *Adv. Phys.* **1964**, *13*, 193–323. [[CrossRef](#)]
3. Pande, C.S. Strain hardening in FCC metals and alloys. *Mater. Sci. Eng.* **2001**, *A309–A310*, 328–330. [[CrossRef](#)]
4. Cottrell, A.H. Commentary: A brief review on work hardening. *Dislocations Solids* **2002**, *11*, vii–xvii.
5. Zepeda-Ruiz, L.A.; Stukowski, A.; Ooppelstrup, T.; Bertin, N.; Barton, N.A.; Freitas, R.; Bulatov, V.V. Atomic insights into metal hardening. *Nat. Mater.* **2021**, *5*, 315–320. [[CrossRef](#)]
6. Hirsch, P.B.; Horne, R.W.; Whelan, M.J. Direct observations of the arrangement and motion of dislocations in aluminum. *Philos. Mag.* **1956**, *1*, 677–684, reprinted in Special Issue: 50 years of TEM of dislocations, *Philos. Mag.* **2006**, *86*, 4553–4572.
7. Mott, N.F. The Work Hardening of Metals. *Trans. TMS-AIME* **1960**, *218*, 962–968.
8. Armstrong, R.W. Plasticity: Grain Size Effects III. In *Reference Module in Materials Science and Materials Engineering*; Hashmi, S., Ed.; Elsevier: Oxford, UK, 2016; pp. 1–23.
9. Armstrong, R.W.; Li, Q.-Z. Dislocation mechanisms of high-rate deformations. *Metall. Mater. Trans. A* **2014**, *46A*, 4438–4453.
10. Kurukuri, S.; Worswick, M.J.; Tari, D.G.; Misra, R.K.; Carter, J.T. Rate sensitivity and tension-compression asymmetry in AZ31B magnesium alloy sheet. *Philos. Trans. R. Soc. A* **2014**, *372*, 20130216. [[CrossRef](#)]
11. Xie, Q.; Zhu, Z.; Kang, G.; Yu, C. Crystal plasticity-based impact dynamic constitutive model of magnesium alloy. *Int. J. Mech. Sci.* **2016**, *119*, 107–113. [[CrossRef](#)]
12. Conrad, H.; Armstrong, R.W.; Wiedersich, H.; Schoeck, G. Thermally-activated Glide in Magnesium Crystals from 4.2 to 420 K. *Philos. Mag.* **1961**, *6*, 177–188. [[CrossRef](#)]
13. Frank, F.C.; Nicholas, J.F. Stable dislocations in the common crystal lattices. *Philos. Mag.* **1953**, *44*, 1213–1235. [[CrossRef](#)]
14. Hirth, J.P. On dislocation reactions in the fcc lattice. *J. Appl. Phys.* **1961**, *32*, 700–706. [[CrossRef](#)]

15. Hansen, N. Effect of grain size and strain on the tensile flow stress of aluminum at room temperature. *Acta Metall.* **1977**, *25*, 863–869. [[CrossRef](#)]
16. Hansen, N.; Ralph, B. The Strain and Grain Size Dependence of the Flow Stress of Copper. *Acta Metall.* **1982**, *30*, 411–417. [[CrossRef](#)]
17. Hall, E.O. The deformation and ageing of mild steel: Discussion of results. *Proc. Phys. Soc. Lond. B* **1951**, *64*, 747–753. [[CrossRef](#)]
18. Petch, N.J. The cleavage strength of polycrystals. *J. Iron Steel Inst.* **1953**, *174*, 25–28.
19. Zerilli, F.J.; Armstrong, R.W. Dislocation-mechanics-based constitutive equations for material dynamics calculations. *J. Appl. Phys.* **1987**, *61*, 1816–1825. [[CrossRef](#)]
20. Zerilli, F.J. Dislocation mechanics based constitutive relations. *Metall. Mater. Trans. A* **2004**, *35A*, 2547–2555. [[CrossRef](#)]
21. Zerilli, F.J.; Armstrong, R.W. Description of tantalum deformation behavior by dislocation mechanics based constitutive relations. *J. Appl. Phys.* **1990**, *68*, 1580–1591. [[CrossRef](#)]
22. Hoge, K.G.; Mukherjee, A.K. Temperature and strain rate dependence of flow stress of tantalum. *J. Mater. Sci.* **1977**, *12*, 1666–1672. [[CrossRef](#)]
23. Peeters, B.; Bacroix, B.; Teodosiu, C.; Van Houtte, P.; Aernoudt, E. Work-Hardening/Softening Behavior of BCC Polycrystals during Changing Strain Paths: II. TEM Observations of Dislocation Sheets in an IF Steel during Two-Stage Strain Paths and Their Representation in Terms of Dislocation Densities. *Acta Mater.* **2001**, *49*, 1621–1632. [[CrossRef](#)]
24. De Mesemaeker, J.; Verlinden, B.; Van Humbeeck, J. On the strength of boundaries in submicron IF steel. *Mater. Lett.* **2004**, *58*, 3782–3786. [[CrossRef](#)]
25. Madec, R.; Kubin, L.P. Dislocation strengthening in FCC metals and in BCC metals at high temperatures. *Acta Mater.* **2017**, *126*, 166–173. [[CrossRef](#)]
26. Messner, M.C.; Rhee, M.; Arsenlis, A.; Barton, N.R. A crystal plasticity model for slip in hexagonal close packed metals based on discrete dislocation simulations. *Model. Simul. Mater. Sci. Eng.* **2017**, *25*, 044001. [[CrossRef](#)]
27. Mishra, A.; Alankar, A. Revisiting dislocation reactions and their role in uniaxial deformation of copper single crystal micro-pillars. *Model. Simul. Mater. Sci. Eng.* **2019**, *27*, 055010. [[CrossRef](#)]
28. Li, Z.; Cui, Y.; Yan, W.; Zhang, D.; Fang, Y.; Chen, Y.; Yu, Q.; Wang, G.; Ouyang, H.; Fan, C.; et al. Enhanced strengthening and hardening via self-stabilized dislocation network in additively manufactured metals. *Mater. Today* **2021**, *50*, 79–88. [[CrossRef](#)]
29. Muñoz, J.A.; Higuera, O.F.; Cabrera, J.M. Microstructural and mechanical study in the plastic zone of ARMCO iron processed by ECAP. *Mater. Sci. Eng. A* **2017**, *697*, 24–26. [[CrossRef](#)]
30. Brown, L.M. Unifying concepts in dislocation plasticity. *Philos. Mag.* **2005**, *85*, 2989–3001. [[CrossRef](#)]
31. Brown, L.M. Constant intermittent flow of dislocations: Central problems in plasticity. *Mater. Sci. Tech.* **2012**, *28*, 1209–1232. [[CrossRef](#)]
32. Alhafez, I.A.; Ruestes, C.J.; Bringa, E.M.; Urbassek, H.M. Influence of pre-existing plasticity on nano-indentation—An atomistic analysis of the dislocation fields produced. *J. Mech. Phys. Sol.* **2019**, *132*, 103674.
33. Goel, S.; Cross, G.; Stukowski, A.; Gamsjäger, E.; Beake, B.; Agrawal, A. Designing nanoindentation simulation studies by appropriate indenter choices: Case study on single crystal tungsten. *Comput. Mater. Sci.* **2018**, *152*, 196–210. [[CrossRef](#)]
34. Armstrong, R.W.; Elban, W.L. Dislocation Reaction Mechanism for Enhanced Strain Hardening in Crystal Nano-indentations. *Crystals* **2020**, *10*, 9. [[CrossRef](#)]